

Synchronization in Hybrid Neuronal Networks of the Hippocampal Formation

Theoden I. Netoff,¹ Matthew I. Banks,² Alan D. Dorval,¹ Corey D. Acker,¹ Julie S. Haas,¹ Nancy Kopell,³ and John A. White¹

¹Department of Biomedical Engineering and ³Department of Mathematics, Center for BioDynamics, Center for Memory and Brain, Boston University, Boston, Massachusetts; and ²Department of Anesthesiology, University of Wisconsin, Madison, Wisconsin

Submitted 20 September 2004; accepted in final form 31 October 2004

Netoff, Theoden I., Matthew I. Banks, Alan D. Dorval, Corey D. Acker, Julie S. Haas, Nancy Kopell, and John A. White. Synchronization in hybrid neuronal networks of the hippocampal formation. *J Neurophysiol* 93: 1197–1208, 2005. First published November 3, 2004; doi:10.1152/jn.00982.2004. Understanding the mechanistic bases of neuronal synchronization is a current challenge in quantitative neuroscience. We studied this problem in two putative cellular pacemakers of the mammalian hippocampal theta rhythm: glutamatergic stellate cells (SCs) of the medial entorhinal cortex and GABAergic oriens-lacunosum-moleculare (O-LM) interneurons of hippocampal region CA1. We used two experimental methods. First, we measured changes in spike timing induced by artificial synaptic inputs applied to individual neurons. We then measured responses of free-running hybrid neuronal networks, consisting of biological neurons coupled (via dynamic clamp) to biological or virtual counterparts. Results from the single-cell experiments predicted network behaviors well and are compatible with previous model-based predictions of how specific membrane mechanisms give rise to empirically measured synchronization behavior. Both cell types phase lock stably when connected via homogeneous excitatory-excitatory (E-E) or inhibitory-inhibitory (I-I) connections. Phase-locked firing is consistently synchronous for either cell type with E-E connections and nearly anti-synchronous with I-I connections. With heterogeneous connections (e.g., excitatory-inhibitory, as might be expected if members of a given population had heterogeneous connections involving intermediate interneurons), networks often settled into phase locking that was either stable or unstable, depending on the order of firing of the two cells in the hybrid network. Our results imply that excitatory SCs, but not inhibitory O-LM interneurons, are capable of synchronizing in phase via monosynaptic mutual connections of the biologically appropriate polarity. Results are largely independent of synaptic strength and synaptic kinetics, implying that our conclusions are robust and largely unaffected by synaptic plasticity.

INTRODUCTION

Cortical oscillations represent locally synchronous activity and may play critical roles in perception and cognition (Fries et al. 1997; Gray et al. 1989; Roelfsema et al. 1997; Winson 1978). In the hippocampal formation, temporally coherent rhythmic activity over a range of frequencies has been observed (Bragin et al. 1999; Burchell et al. 1998; Chrobak and Buzsáki 1998; Fellous and Sejnowski 2000; Konopacki et al. 1987; Traub et al. 1999; Whittington et al. 1995; Ylinen et al. 1995), but the cellular and synaptic mechanisms underlying these rhythms are not fully elucidated. This elucidation is difficult because these behaviors depend on the interaction of many neurons with distinct cellular populations and patterns of

connectivity in different subregions (Freund and Buzsáki 1996; Gloor 1997). Our ability to record from large numbers of neurons simultaneously, with single-cell resolution, is limited. Instead, we can build an understanding of the network dynamics from the dynamics of the individual components within the network. Such single-cell measurements can be used to construct network models that make specific predictions, which in turn can be tested by coupling pairs of neurons under dynamic clamp.

Two complementary modeling approaches have been used to study the mechanistic underpinnings of synchronous neural activity. One uses detailed biophysical models (e.g., Lytton and Sejnowski 1991; Traub et al. 1996; Wilson and Bower 1992) to reproduce aspects of the observable voltage dynamics. The second method uses much more simplified models to get insight into what aspects of the intrinsic and synaptic currents play critical roles in the observed dynamics. Some studies based on the second, simplified approach focus on networks with weak coupling (e.g., Hansel et al. 1995; Kopell and Ermentrout 2002; Van Vreeswijk et al. 1994). This paper, like a number of other studies (e.g., Acker et al. 2003; Canavier et al. 1997; Chow et al. 1998; Demir et al. 1997; Ermentrout and Kopell 1998; Kopell and Ermentrout 2002), concentrates on the effects of single spikes on the timing of the downstream cells without making explicit use of the assumption of weak coupling. For this purpose, we introduce a refined experimental technique, the *spike time response* (STR) method, that can be used to build tractable and testable models of network function from recordings of single neurons.

The STR technique is an experimental implementation based on methods that have been proposed theoretically for studying synchronization among such oscillators (e.g., Acker et al. 2003; Canavier et al. 1997; Hansel et al. 1995; Kopell and Ermentrout 2002; Van Vreeswijk et al. 1994; Winfree 2001). We dispense with the assumption of weak coupling, which our previous work (Acker et al. 2003) indicates does not hold in our circumstances. We use the dynamic-clamp technique (Dorval et al. 2001; Robinson and Kawai 1993; Sharp et al. 1993) to measure the spike time response curve (STRC) in response to directly applied artificial synaptic inputs. The advance or delay is a function (described in the STRC) of the time of the most recent input relative to the most recent previous spike of the cell. The central idea is that if the next spike of the cell in question depends only on this recent history, the STRC contains all the information necessary to predict synchronization behavior. In that sense, this method is a bridge between

Address for reprint requests and other correspondence: J. A. White, Dept. of Biomedical Engineering, Boston University, 44 Cummings St., Boston, Massachusetts 02215 (E-mail: jwhite@bu.edu).

The costs of publication of this article were defrayed in part by the payment of page charges. The article must therefore be hereby marked "advertisement" in accordance with 18 U.S.C. Section 1734 solely to indicate this fact.

biophysics and dynamics: knowing the STRC is enough to predict the synchronization behavior, and information about membrane properties helps explain the shape of the STRC (Acker et al. 2003; Crook et al. 1998; Demir et al. 1997; Ermentrout et al. 2001). The central assumption that only recent history matters is easily testable from our experimental data and holds well.

The current paper employs an experimental technique that allows one to measure the STRC associated with a given cell and a given stereotypic conductance input and to use this measurement to predict the synchronization of that cell with another. Relative to other experimental studies of STRCs (Reyes and Fetz 1993; Stoop et al. 2000), our method has three advantages. First, we use the dynamic-clamp technique (Dorval et al. 2001; Robinson and Kawai 1993; Sharp et al. 1993) to apply well-controlled conductance inputs as opposed to relying on current pulses or variable inputs driven by shocking presynaptic fibers. Second, we monitor and carefully control the baseline firing rate of the cell. Controlling average rate allows us to prevent nonstationarities in firing rate from corrupting the normal, cycle-to-cycle variability. Third, we use STRCs to predict phase relationships in hypothetical networks of mutually coupled neurons and test these predictions by coupling recorded cells to biological or computationally modeled counterparts to create *hybrid networks*. Invariably, we find that predictions from STRCs hold up well in the hybrid networks.

The particular cells that we study in this paper are the stellate cells (SCs) of the medial entorhinal cortex, which have received much modeling attention (Acker et al. 2003; Dickson et al. 2000; Fransen et al. 2002; Hasselmo et al. 2000; White et al. 1995, 1998b), and the oriens lacunosum/moleculare (O-LM) cells of the hippocampus. Both cells display autonomous theta frequency oscillations (Alonso and Llinás 1989; Gillies et al. 2002; Pike et al. 2000), and both are known to express slow, hyperpolarization-activated currents that are believed to contribute to the oscillations (Dickson et al. 2000; Maccaferri and McBain 1996). Earlier modeling work (Acker et al. 2003) has shown that such cells can be expected to synchronize with excitation, but not with inhibition, in contrast to other neurons not possessing this current. This is the motivation for using SCs and O-LM cells: though they release different neurotransmitters (SCs release glutamate and O-LM cells release GABA), they are thought to have similar intrinsic currents, and one expects from previous models that they will behave in similar ways to interaction through excitation or inhibition. The dynamic-clamp methodology allows one to test this and show that they do indeed have similar synchronization properties. These results imply that SCs, but not O-LM interneurons, are capable of in-phase synchronization through mutual, monosynaptic connections of their natural "sign" (excitatory for SCs, inhibitory for O-LM cells).

The dynamic-clamp method allows one to look at other pairings that are not native to either set, including excitatory-inhibitory (E-I) and inhibitory-excitatory (I-E). The point of this exercise is to test the ability of the STRCs to predict synchronization behavior. We show that the predictions can match not only the qualitative behavior but also the quantitative behavior in complex dynamics (such as temporary locking and phase walk-through). Indeed, the measured STRCs, which include noise, can predict not just whether or not a pair will

lock, but the histograms of the resulting phase differences as well.

METHODS

Physiology

All experiments were conducted as approved by the Boston University Institutional Animal Care and Use Committee and the University of Wisconsin Research Animals Resource Committee. Measurements from SCs of the medial entorhinal cortex, the input structure of the hippocampal formation, were made at Boston University. Measurements from O-LM cells of hippocampus were made at the University of Wisconsin. Long-Evans (for MEC experiments) and Sprague-Dawley (for hippocampal experiments) rats, 14–21 days old, were anesthetized with CO₂ or isoflurane and decapitated. The brain was removed and chilled in ACSF [which contained (in mM) 126 NaCl, 1.25 NaH₂PO₄, 1.4–2 MgSO₄, 26 NaHCO₃, 10 dextrose, 3 KCl and 2 CaCl₂] and then sliced using a Vibratome to 350 μ m thickness. After letting slices recover for ≥ 1 h in a holding chamber, we transferred slices to a heated (34–36°C) chamber (Warner Instruments), mounted on a microscope stage. Slices were perfused with heated ACSF. In most cases, 4 mM kynurenic acid and 10 μ M bicuculline (Sigma) were added to block ionotropic excitation and inhibition, respectively. However, results were not altered by spontaneous synaptic events. Neurons within slices were visualized using dual-interference contrast video microscopy (Zeiss AxoSkop FS2, Dage/MTI CCD camera). Whole cell patch-clamp recordings were obtained using patch pipettes (4–6 M Ω) fabricated from borosilicate glass (1.0 OD, 0.75 ID, Sutter Instruments) and filled with (in mM) 135 K-gluconate, 2 MgCl₂, 2 (MEC) or 10 (O-LM cells) NaCl, 1.25 (SCs) or 0.1 (O-LM cells) EGTA, 10 HEPES, 2 Tris-ATP, and 0.4 Tris-GTP (SCs). Differences in the strain of rats used, and in the intracellular solution, are due to unimportant differences in the default choices of the two labs. Biocytin (0.3%) was used in O-LM recordings to allow later morphological reconstruction. Biocytin was not used in recordings from SCs because they are easily identifiable by electrophysiological criteria (Klink and Alonso 1997) and because we found that use of biocytin led to significant spike broadening in SCs, consistent with previous results from other cellular populations (Eckert et al. 2001; Schlosser et al. 1998; Xi and Xu 1996).

In MEC slices, recordings of stellate cells (SCs) were made from the cell-dense layer 2. Stellate cells were identified electrophysiologically using established criteria, based on the presence of a large, slow inward rectifying cation current as seen under current clamp (Alonso and Klink 1993). We measured 67 neurons from 48 slices taken from 28 rats. Of these neurons, 56 neurons were identified as SCs according to the physiological criteria (large "sag" current, small 1st-spike latency) of Alonso and Klink (1993). Only SCs were included in the rest of this study.

Recordings from hippocampal interneurons were made in stratum oriens. A total of 15 recordings are included here. Because biocytin did not appreciably broaden action potentials in interneurons, we were able to stain, react, and characterize these cells morphologically in 10 of 15 cases. Eight of 10 identified cells could be characterized as O-LM interneurons based on standard morphological criteria (Freund and Buzsáki 1996). The five unidentified cells had electrophysiological properties that were very similar to those of the identified O-LM cells and were included in the analysis.

Real-time experimental control

A real-time experimental control system (Dorval et al. 2001) was used for a number of manipulations in these experiments, including controlling spike rate, delivering artificial synaptic conductance inputs, and building hybrid neuronal networks. The system is based around real-time versions of the Linux operating system. It is publicly

available and can be downloaded from our website (<http://bme.bu.edu/ndl/>).

RATE CONTROL. STRCs (see following text) are more easily measured and interpreted if the baseline firing rate is kept stationary. We developed an iterative, proportional feedback algorithm to control the firing rate at a user-defined value. The feedback algorithm was used in both STRC measurements and in hybrid network experiments. The spike rate was controlled by measuring the error of the interspike interval and changing the current by an amount proportional to the error. The proportionality constant was changed depending on the history of the error. As long as the error decreased monotonically and remained either positive or negative, the proportionality constant was left unchanged. If the sign of the error changed, then the new proportionality constant was determined using the bisection method. If the error increased, the proportionality constant was doubled. The maximal change in current was capped at 40 pA. By its nature, the algorithm was very conservative, making very small changes unless there were persistent, systematic errors in measured interspike intervals (ISIs). The algorithm's conservative design meant that it did not attempt to control the inherent noise in ISIs of stationary neurons.

When measuring STRCs, the ISI was averaged over five spikes. The artificial synaptic inputs were delivered only once per six firing cycles, and the current was changed one full cycle after the ISI in which the synaptic stimulus was applied. This method allowed us to measure the effects of synaptic stimuli on the two subsequent ISIs without confounding effects of the spike rate controller. In practice, changes in applied current were quite small. For example, in the data associated with Fig. 2A, the average change in applied current was 0.6 ± 1.4 (SD) pA per six ISIs, far smaller than the artificial synaptic currents we delivered (tens to hundreds of pA). In no cases did controller-induced changes in applied current lead to immediate spikes. Our criterion for successful rate control was that no short-term change in applied current was >5 pA. Changes in applied current ranged from 5 to 50 pA over the course of an entire experiment.

We also used the rate controller to keep neurons' spike rates stationary during hybrid network experiments. In this case, the amount of current was adjusted every cycle, again by <1 pA per adjustment. For networks that synchronized, the effect of the rate controller was minimal because in these cases, the cells do not change each others' average rates. For networks that settled into nonsynchronous states, the rate controller reacted to bring the coupled cells back to their baseline rates, which means that the cells had slightly different natural frequencies than during the STRC measurements. The fact that we invariably saw close agreement between predictions from STRCs and results in hybrid networks implies that this confounding effect of the rate controller was small.

STRCS. The STRC represents the amount by which a synaptic input, occurring at a particular time relative to the most recent postsynaptic spike, advances or delays the next postsynaptic spike. STRCs were generated by delivering artificial excitatory or inhibitory conductance inputs (EPSCs or IPSCs, respectively) to periodically firing neurons, and measuring induced changes in spike timing. EPSCs and IPSCs were generated using a dynamic-clamp system (Dorval et al. 2001) and delivered once every six cycles of periodic firing. This protocol allowed us to track and control the baseline firing rate (i.e., the rate with no synaptic input delivered) and to collect enough baseline intervals for statistical comparisons.

The dynamic clamp generated a signal of form $I_s = G_s(e^{-t/\tau_{fall}} - e^{-t/\tau_{rise}})(V_m - V_s)$, where G_s is the maximal synaptic conductance, t is the time since the initiation of the synaptic event, τ_1 is the synaptic decay time constant, τ_2 is the synaptic rise time constant, V_m is membrane potential, and V_s is the synaptic reversal potential. This signal was scaled appropriately, converted to an analog signal, and passed to the current-drive channel of the bridge-balance amplifier (Axon Instruments Axoclamp 2B or Multiclamp 200A). The mea-

sured value of V_m was updated, and a new value of I_s calculated and delivered at a clock rate of 5–10 kHz.

STRCs might be expected to change as the amplitude and time constants of the synaptic conductances are varied. For most measurements, we used inputs of peak amplitude 1 nS, 4–5 times the size of spontaneous excitatory synaptic inputs to SCs as measured in the literature (Berretta and Jones 1996) and 8–10 times the size of "miniature" conductance changes corresponding to release of single quanta (data not shown). Our use of larger synapses in this work is justified because we would expect multiple inputs to arrive simultaneously during the often highly structured activity seen in entorhinal cortex and hippocampus. In our "small networks" approach, each cell represents a synchronized population and thus should induce larger-than-unitary conductance changes. Nevertheless, for drawing general conclusions, it is important to show that our results do not depend strongly on synaptic strength, which is likely to exhibit short-term plasticity at any cortical synapse (Markram et al. 1998; Thomson and Deuchars 1994). In some experiments (Fig. 4A), we varied the amplitude of our EPSCs and IPSCs from 0.1 to 1 nS, ranging from the amplitude of a single quantal release to ~ 10 quantal releases for excitatory inputs to SCs; network synchronization predicted from the measured STRCs was largely independent of synaptic strength.

Time constants describing synaptic rise and fall at the cell body can differ considerably from case to case based on factors like the location of the synapse relative to the soma (Berretta and Jones 1996; Spruston et al. 1994) as well as both the subunit composition and the alternative splicing state of the receptor (Jonas 2000). Additionally, the kinetics of a given postsynaptic receptor may be modified via phosphorylation (Hinkle and Macdonald 2003). For most experiments, we used stereotypical time constants corresponding to synapses near the somatic recording site: $\tau_{rise} = 1$ ms and $\tau_{fall} = 2$ ms for EPSCs, $\tau_{rise} = 1$ ms and $\tau_{fall} = 4$ ms for IPSCs. These values gave somewhat faster kinetics than those observed for spontaneous EPSCs to SCs measured in stellate neurons (Berretta and Jones 1996). To verify that our results were not dependent on the subtleties of the synaptic kinetics, we measured STRCs while varying modeled synaptic kinetics but preserving the total integrated synaptic conductance (Fig. 4B).

HYBRID NETWORKS. STRCs can be used to predict phase relationships in simple networks. To test these predictions, we constructed two types of hybrid networks:

First was networks composed of one biological neuron and one "virtual" counterpart. In this case, a real-time algorithm detected spikes in the biological cell. The virtual cell was represented by a STRC capturing the typical behavior in the biological population being studied or, in some cases, the STRC of the particular cell being studied. Spike events in virtual cells were generated by selecting a spike time exactly one period after the last virtual spike event, then adjusting this event time by an amount determined from the STRC, evaluated at the biological neuron's spike time relative to the last virtual spike. For these experiments, the next spike time in the virtual cell does not include a stochastic component. Spike events in the virtual cell drove conductance changes (see preceding section) in the biological cell, beginning after a delay of one time step (0.1 ms). In some cases, an additional synaptic delay of 0.5 ms was added; results did not depend on this detail. In some cases, we studied *unilaterally* coupled networks, in which the modeled cell inhibited the biological cell but not vice versa. For these cases, we focused on unilateral inhibition because we wanted to see if the cells could stably phase lock to the periodic inhibitory drive as would be predicted for many classes of cells that synchronize via mutual excitation (Acker et al. 2003).

Second was networks composed of two biological neurons coupled by "virtual" chemical synapses. In this case, spikes detected in either biological cell drove artificial synaptic conductance changes in the cell's counterpart. The minimal time lag between spike detection and beginning of the application of the postsynaptic conductance change

was ensured by the real-time dynamic clamp system to be one time step (0.1 ms). As before, synaptic delays of 0.5 ms were added in some cases without changing the results.

Curve fitting, iterative spike timing simulations, and data analysis

The average values of spike time responses were fit using a polynomial function of time to create an STRC. For excitatory responses, the polynomial was of the form $t(ISI - t)(At^3 + Bt^2 + Ct + D)$, where t is the time since the last spike, ISI is the interspike interval (i.e., $1/\text{target firing rate}$), and A – D are free parameters. This fitting function ensured that the curve had zeroes at its left and right extremes, compatible with the trends in our data. For inhibitory responses, the polynomial had the form $t(At^3 + Bt^2 + Ct + D)$. In this case, we did not “pin” the polynomial to a value = 0 at $t = \text{ISI}$ because such trends were usually not seen in the data. The SD of the data was fit using a statistical procedure with multiple steps. First, we subtracted out the time-dependent average. Second we fit the distribution using a maximum likelihood fit to a Gaussian distribution with time-dependent SD $E(1 - t/\text{ISI})^{-1/2} + F$, where t and ISI are defined as in the preceding text and E and F are free parameters. This procedure allowed us to fit the scatter for excitatory inputs for which we observed that SD decreases proportional to $t^{-1/2}$; and inhibitory inputs for which SD is largely independent of the time of the input.

Predictions of time differences in two-cell networks were made using an iterative, algebraic algorithm that predicts future spike times in terms of baseline firing period and the STRC (mean \pm SD). The algorithm was seeded with a randomly chosen, nonsynchronous initial condition. In subsequent iterations, firing times for each cell were chosen by adding the STRC value (mean + normally distributed random component scaled by the time-dependent SD, each measured from the STRC) to the unperturbed firing period of the cell in question.

Predicted histograms of spike timing differences were compared directly with measured results from hybrid networks using a χ^2 test. Means and SD of the spike time difference histograms were measured by converting the spike time differences to unit vectors in which the angle represents the normalized difference in phase of the two spike times. The mean spike time difference was calculated by summing these unit vectors, then converting the phase of the summed vectors back into units of ms (Figs. 4 and 5) or normalized time (time divided by the average interspike interval, Fig. 6; this method allows us to compare data collected at different spike rates). We characterized the amount of spread in spike time difference histograms using two measures: first, σ is the estimated SD in spike time differences. In performing this calculation, we used only spike time differences within \pm a half-cycle of the mean spike time difference, to avoid confounding effects due to the circular nature of phase. Second λ is the percentage of “inliers.” λ is a direct measure of the number of spike time differences, normalized by the average ISI, that fall within $\pm 10\%$ of the mean spike time difference. The purpose of this measure was to determine the proportion of time that the cells were settled into a preferred phase-locked state. σ is not always a good measure of phase-locking because phase-slipping in two-cell networks often leads to long tails in the distributions of spike time differences.

RESULTS

Predicting synchronization properties

To investigate the ability of entorhinal SCs and CA1 O-LM interneurons to participate in synchronous firing patterns, we use tonic excitatory current to cause the cells to fire periodically

at 100- to 150-ms intervals (6.7–10 Hz). Under dynamic clamp, we next induce artificial, excitatory or inhibitory synaptic conductance inputs (EPSCs or IPSCs) in the targeted neuron (Fig. 1). Depending on the time of occurrence of the input (an EPSC in Fig. 1), subsequent spikes may be advanced or delayed. Artificial conductance inputs are delivered at a randomly chosen time once every six cycles. These conductances are typically 1 nS at peak and induce 1- to 4-mV changes in membrane potential. Unperturbed ISIs are measured to monitor spike rate drift. If necessary, constant current applied to the cell is adjusted to keep the baseline firing rate constant. In post hoc data analysis, we compare unperturbed ISIs with intervals perturbed by E/IPSCs. From hundreds of such measurements, we obtain STRCs, which allow us to quantify the mean and variance of changes in spike timing induced by EPSCs (Fig. 2A) or IPSCs (Fig. 2B) as functions of input timing. In our corpus of data, the shapes of STRCs were consistently similar from cell to cell and did not depend strongly on firing rate for interspike intervals from 80 to 150 ms. Responses to “early” inputs were invariably noisy (as seen in Fig. 2), with a SD of ~ 10 ms. The SD of the ISI for control (unstimulated) intervals was also 10–12 ms, implying that the jitter in the spike time advance was due to inherent variability in the ISI under stationary conditions, rather than noisy effects of the synaptic stimulus. “Late” excitatory inputs lead to almost immediate spikes, the timing of which was more tightly distributed than that of spikes generated by early inputs.

In SCs and O-LM interneurons, artificial E/IPSCs induce significantly larger changes in spike timing for the cycle during which the input occurs (points and solid lines in Fig. 2, which we refer to as the STRC) than for subsequent cycles (dashed lines in Fig. 2 represent residual effects on spike timing during the next cycle). In some models, it has been shown that such residual effects can be important (Oprisan and Canavier 2001).

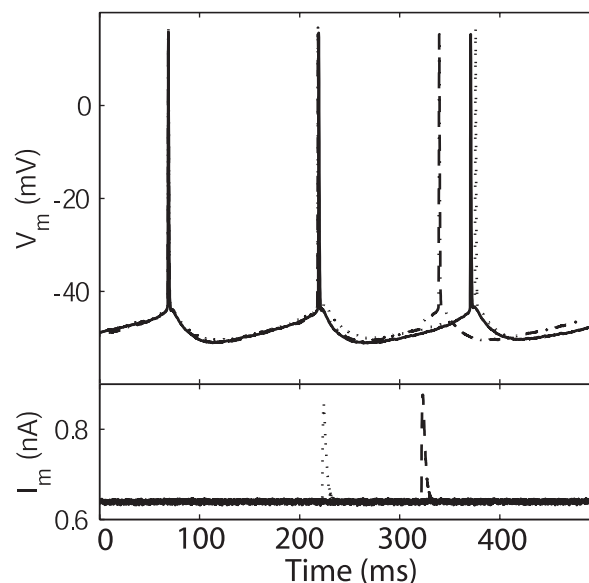


FIG. 1. Time-dependent effects of an artificial excitatory postsynaptic conductance (EPSC) input on spike timing in a regularly firing stellate cell (SC). Voltage traces are shown at top with corresponding current traces at bottom. Solid lines, periodic firing (at 150-ms intervals) in a neuron receiving no EPSC. Dotted lines, a delay induced by an artificial EPSC introduced early in the interspike interval (ISI). Dashed lines, the same artificial EPSC, introduced late in the ISI, advances the next spike.

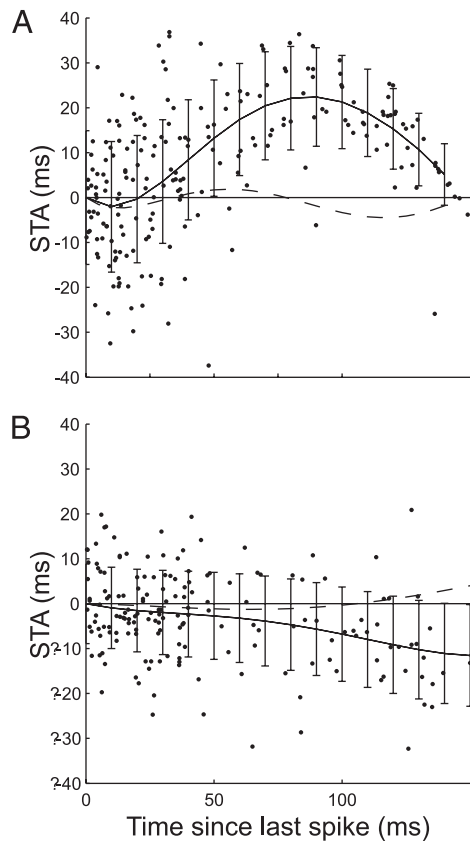


FIG. 2. Spike time response curves (STRCs) measured from a SC in the medial entorhinal cortex. STRCs represent measurements of hundreds of perturbations to the expected spike times of periodically firing neurons. Perturbations from the unperturbed period (150 ms in this case) are measured as the spike time advance (STA, y axis), plotted vs. the time of the EPSC (A) or inhibitory PSC (IPSC, B). In both cases, the peak conductance change was 1 nS. The solid lines indicate the best least-squares fit of a polynomial function to the data. Time-dependent SDs (error bars) were curve-fit as well. Residual changes in average spike timing for the 2nd spike after the stimulus (dashed lines) are smaller than the STRCs (solid lines).

In our analysis, we will show that one can obtain accurate predictions of network behavior without accounting for residual effects.

The advantage of considering only the primary STRC is that it allows one to predict the behavior of mutually coupled networks using simple algorithms and reasoning. Consider a hypothetical two-cell network with mutual excitatory coupling, in which the effects of each cell on the other are described by the STRC in Fig. 2A. If two mutually coupled cells with identical firing periods $T = 150$ ms are started in a randomly chosen state, one cell will necessarily receive input in the time range 0–75 ms, assuming that the cells are neither perfectly synchronous nor perfectly anti-synchronous. We refer to this as the “leading” cell. The “trailing” cell receives input during the time range 75–150 ms. With STRCs that have a greater mean advance in the second half the interval than the first, the trailing cell will tend to be advanced more than the leading cell. The net effect of mutual coupling will be synchronizing: the leading cell will, on average, receive its next input closer to $t = 0$, and the later trailing cell will receive its input closer to $t = 150$ ms. Over time, the cells will come very close to synchronous firing. One can apply similar reasoning to predict the behavior of mutually inhibitory networks using data from Fig. 2B. In this

case, if the cells start in the nearly synchronous state, the leading cell should be delayed less than the following cell. Thus spike time differences will tend to grow, implying that this mutually inhibitory network will not synchronize stably in phase. Instead, the cells will phase lock when they are separated by half the ISI. At this point in time, the delays are equal for the two cells, implying that the cells will phase-lock stably, in anti-phase, at a firing rate that is slightly smaller than each cell’s baseline rate.

This heuristic argument can be formalized rather straightforwardly. For noiseless STRCs, the formal argument involves mathematically combining two STRCs and looking for mutually compatible solutions (Acker et al. 2003; Canavier et al. 1997; Oprisan and Canavier 2002; Oprisan et al. 2003). While this method predicts the mean phase difference, it does not predict the variability around that phase that occurs with real-world, noisy STRCs. To predict the variability, we perform iterative simulations (described in METHODS) of two “cells” that affect each others’ spike timing via STRCs. We start these two simulated cells in a randomly chosen, nonsynchronous state, then we update the firing time of each, using the STRC with a noisy component. Over hundreds of iterations, we build a histogram of spike timing differences between the two simulated cells. These histograms of spike time differences (e.g., the solid lines in the *rightmost column* of Fig. 3) serve as predictions of network behavior in mutually coupled, two-cell networks.

Synchronization and phase locking in hybrid networks

The power of spike time response curves lies in their ability to predict phase relationships in interconnected neuronal networks. We tested these predictions by constructing two types of hybrid neuronal networks: those containing one biological and one “virtual” counterpart, modeled in real-time by a computer, and reflecting the typical behavior seen in a given cell type; and those containing two biological neurons, coupled by real-time, computer-controlled virtual synapses (see METHODS for more detailed descriptions of hybrid networks). To test the STRC’s ability to predict the dynamics of many networks of different forms, we connected the cells in several different ways. Figure 3A shows results from the biological-virtual neuron network coupled in four different ways: with mutual excitation (E-E) as one would expect from monosynaptically coupled SCs; mutual inhibition (I-I), as one would expect for SCs that communicate via GABAergic intermediaries (although we ignore associated delays in such polysynaptic circuitry; these delays would be of order 1–5 ms, still quite small compared with the firing period); unilateral inhibition (O-I), in which the virtual cell inhibits the biological cell, with no effect in the opposite direction (amounting to periodic inhibition at the forcing cell’s baseline firing rate); and mixed excitation (from the biological cell) and inhibition (from the virtual cell) (E-I). Plots show rasters of spike time differences plotted versus spike number. These rasters were calculated by finding and plotting the spike times of the two spikes in the biological cell that lay nearest each spike in the virtual cells. The histograms at right show summary data for the entire data trace. The E-E network generates stable synchrony, indicated by a time difference near 0 ms, with modest variance. Occasional departures from synchronous firing are small and corrected within a

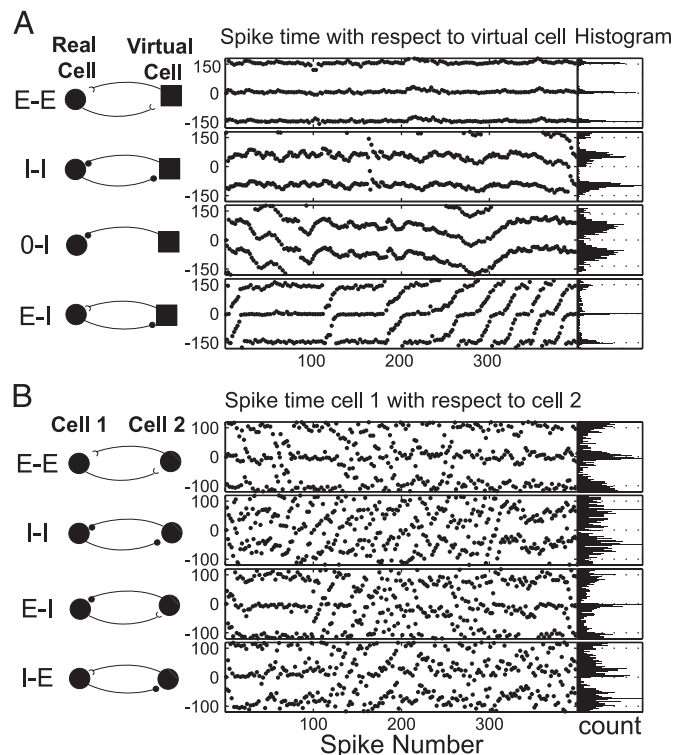


FIG. 3. Free-running hybrid networks. *A*: spike times of a biological SC, firing at 100-ms intervals, with respect to its virtual counterpart, plotted versus spike number. Four types of networks were constructed: E-E (mutual excitation), I-I (mutual inhibition), 0-I (periodic inhibitory drive from the virtual cell with no feedback), and E-I (excitatory biological cell, inhibitory virtual cell). In the middle column, the spike time difference is plotted against the spike number. *Time 0* on the y axis indicates the firing time of the virtual neuron; points represent the relative firing times of the biological cell to the virtual neuron. Times are in milliseconds; times below 0 ms imply that the spike in the biological cell preceded that in the virtual cell. In the rightmost column are histograms of the spike time differences. *B*: spike times of 1 biological SC with respect to another in 4 types of networks: E-E (mutual excitation), I-I (mutual inhibition), E-I (*cell 1* excitatory, *cell 2* inhibitory), and I-E (*cell 1* inhibitory, *cell 2* excitatory). Raster plots in the center panels show timing of spikes in *cell 1* with respect to each spike in *cell 2*. Histograms at right show summaries of all spike time differences.

few cycles. The I-I network generates stable spike time differences that are nearly anti-synchronous, have greater variance, and self-correct more slowly than in the E-E network. These results are consistent with modeling work (Acker et al. 2003) that predicted that SCs, which express a significant amount of the slow inward rectifier I_h , should synchronize better through mutual excitation than through mutual inhibition.

“Heterogeneous” 0-I and E-I networks behave somewhat differently from “homogeneous” E-E and I-I networks. For the 0-I network, the biological cell tends to fire out of phase with the virtual cell. These data show slow trends in the spike time differences (e.g., in the region of spike number 200–300 in the 0-I network of Fig. 3*A*). These slow trends may include contributions of “beating” between virtual and biological cells due to a mismatch in frequency caused by small error (of 1–2%) in spike rate control, but there are other mechanisms at play. The E-I network (Fig. 3*A*, row 4) often fires nearly synchronously but undergoes occasional bouts of “phase slipping” (seen between spikes 110 and 120). The raster plots indicate that phase slipping arises when a phase-locked state is stable when one cell leads but not the other. In this case, the

network is stable when the excitatory cell leads the inhibitory cell (indicated by negative values of the time difference), but phase slips whenever noise reverses this leader-follower relationship (for more on phase slipping, see Fig. 5 and the DISCUSSION). Because frequency mismatches in these experiments are quite small (around 1%), the phase-slipping in the E-I network is too fast to be generated by “beating” (i.e., the situation in which the two cells are firing periodically and independently at phase differences that change slightly with each cycle due to consistent differences in firing rate). Instead, phase-slipping is caused because the inhibitory cell cannot stably lead the excitatory cell; cycle by cycle, the inhibitory cell will delay the excitatory cell until the E-cell has skipped one entire cycle and begins to fire just before the inhibitory cell. At this point, the network will stabilize again.

Figure 3*B* shows results from the second type of hybrid network, in which two biological SCs are mutually coupled in 4 different ways: with mutual excitation (E-E); mutual inhibition (I-I); and mixed excitation (from one of the cells) and inhibition (from the other cell) (E-I or I-E, depending on whether the arbitrarily chosen cell 1 was excitatory or inhibitory). The rastergram plots spike time differences, calculated by finding the times of cell 1 with respect to the spikes in cell 2. These spike time rasters are summarized in the histograms at right. This E-E network generates stable synchrony that is somewhat noisier than in Fig. 3*A*, presumably because both neurons respond inherently noisily. The I-I network generates stable spike time differences that are nearly anti-synchronous and have greater variance than in the E-E network or the simpler, less noisy I-I network from Fig. 3*A*.

The bottom two rows of Fig. 3*B* show responses from “heterogeneous” E-I and I-E networks. Since both of these cells were entorhinal SCs, the distinction between E-I and I-E is arbitrary; they are networks of the same form, and if the neurons were identical the E-I and I-E networks would behave identically. Identical behavior of the network would imply that the E-I and I-E histograms at right would be identical in shape, although rotated around the point $\Delta t = 0$ because cell 2 is “inhibitory” in the E-I case but “excitatory” in the I-E case. In both cases, the network has a preferred spike time difference, with the “excitatory” cell leading the “inhibitory” cell ($\Delta t < 0$ for the E-I network, $\Delta t > 0$ for the I-E network). But the amount of spread in the two histograms is different, because these heterogeneous networks are sensitive to small differences in cellular properties. We will return to this subject, and give quantification of the level of spread in data sets, in our discussion of Figs. 5–6. Clear evidence of phase-slipping is less obvious here than in Fig. 3*A*, presumably because both participants in the networks of Fig. 3*B* are noisy.

Synaptic amplitudes are not static. Both synaptic amplitudes and synaptic kinetics are subject to change due to synaptic plasticity. We explored the effects of these parameters by varying them systematically in individual cells, then calculating predicted synchronization properties in *post hoc* iterative simulations. Figure 4 shows typical data from such experiments performed 6 times. Figure 4*a* shows STRCs and spike time difference histograms generated by excitatory (left column) and inhibitory (right column) inputs that varied from 100 pS (half the size of measured unitary EPSPs (Berretta and Jones 1996)) to 1 nS. For both excitatory (left column) and inhibitory inputs (right column), spike time difference histo-

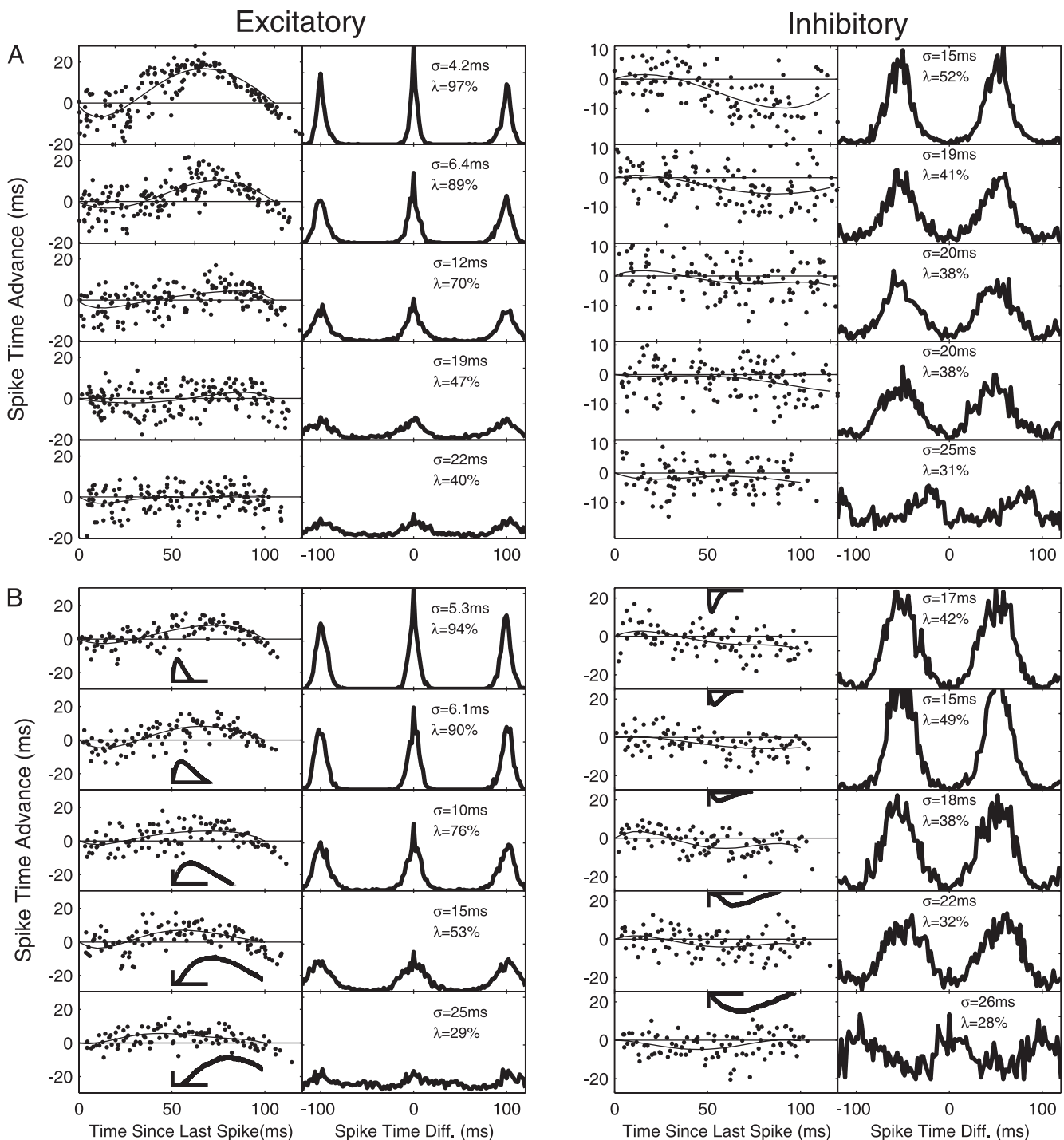


FIG. 4. Changes in STRC as amplitude and time constants of post synaptic conductances (PSGs) are varied. (a) STRCs measured with amplitudes of EPSPs (left column) and IPSPs (right column) that differed in amplitude. The unperturbed period was 100 ms. From top to bottom, peak conductances for both EPSPs and IPSPs were 1 nS, 562 pS, 316 pS, 178 pS, and 100 pS. EPSP rise and fall times were $\tau_{\text{rise}} = 1.68$ ms and $\tau_{\text{fall}} = 6.5$ ms; for the IPSPs, $\tau_{\text{rise}} = 2.5$ ms and $\tau_{\text{fall}} = 5$ ms. The histograms are of simulations of two identical neurons coupled using the STRCs measured. Phase locking can be seen for all but the smallest IPSP amplitude. σ is the SD of the spike time differences, and λ measures the propensity of the network to lie near its preferred, phase-locked state (see METHODS). (b) STRCs measured using different time constants. The area of the conductances were kept the same, while rise, fall and amplitudes were adjusted. The ratios of the rise to fall time were kept constant at 1.68/6.21 for the EPSPs and 2.5/5 for the IPSPs. From top to bottom, values of τ_{fall} were 2 ms, 3.5 ms, 6.2 ms, 11 ms, and 20 ms for EPSPs; and 1.6 ms, 2.8 ms, 5 ms, 8.9 ms, and 16 ms for IPSPs. Insets show evoked PSPs on the same time scale (time bar is 20 ms long and amplitude bar is 1 mV). Simulations of the two cell networks indicate that the STRCs predict comparable results except for the slowest IPSP.

grams were sharper for larger inputs, but mean spike time differences were independent of synaptic size. Only the smallest inhibitory inputs tested failed to generate coherent network activity. It is interesting to note that even STRCs whose

maximum spike time difference is of the amplitude of the noise level (e.g., the 100 pS case for excitatory inputs) can give rise to stable phase relationships. The stable synchrony in this case arises because, despite the noisiness of the STRC, early inputs

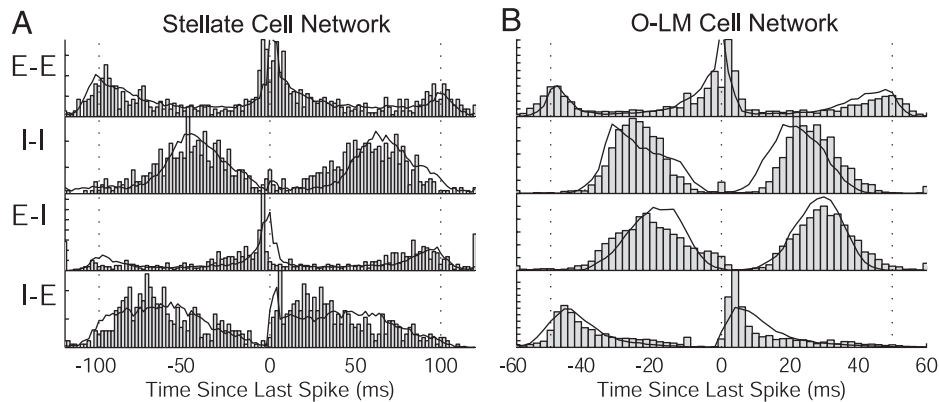


FIG. 5. Observed spike time difference histograms in paired recordings with virtual synapses match predictions from STRCs. Pairs of SCs firing at 100ms intervals (a) and O-LM interneurons firing at 50ms intervals (b) were connected through dynamic clamp. Zero on the x-axis indicates the firing time of cell 1 (arbitrarily chosen). Gray bars indicate where cell 2 fired in relation to cell 1. Four networks were constructed: E-E, I-I, E-I and I-E, where the first letter indicates the “sign” of cell 1’s effects on cell 2, and the second letter indicates that of cell 2’s effects on cell 1. The means (\bar{x} , ms), SDs (σ , ms), and percentage of “inliers” (λ , %) of the observed spike time difference distributions are as follows. For the SC: E-E, $\bar{x}=5.4$, $\sigma=14$, $\lambda=48\%$; I-I, $\bar{x}=58$, $\sigma=15$, $\lambda=35\%$; E-I, $\bar{x}=88$, $\sigma=14$, $\lambda=49\%$; I-E, $\bar{x}=28$, $\sigma=15$, $\lambda=43\%$. For the O-LM interneuron: E-E, $\bar{x}=-0.94$, $\sigma=6.9$, $\lambda=55\%$; I-I, $\bar{x}=25$, $\sigma=6.0$, $\lambda=51\%$; E-I, $\bar{x}=30$, $\sigma=7.0$, $\lambda=37\%$; I-E, $\bar{x}=6.7$, $\sigma=7.0$, $\lambda=62\%$. Solid lines indicate predicted results from iterative simulations based on STRC measurements for the two cells. Predicted and observed distributions are qualitatively similar, although statistically distinguishable at the $P = 0.01$ level (χ^2 test).

($t < 20$ ms) still lead to consistently more negative spike time advances than late inputs ($t > 80$ ms).

Manipulations of the time course of virtual synapses are shown in Fig. 4b, again ranging over an order of magnitude. In these manipulations, peak conductances were scaled to keep total integrated conductance constant. Evoked EPSPs and IPSPs, shown in the insets, do not scale linearly with conductance size because of membrane-induced filtering and nonlinearities. Again, mean spike time differences were largely

insensitive to this manipulation. For the largest values of the inhibitory rising and decay time constants τ_r and τ_f (Fig. 4b, bottom of right column), the predicted effect of mutual inhibition switched from anti-synchronizing to synchronizing. We simulated this network using the primary and the secondary STRCs and found the results did not change (data not shown). This determines that the result was not due to ignoring the effects of the synaptic input on the following ISI and confirms that this result is due to a change in the cell’s response to slow synaptic inputs.

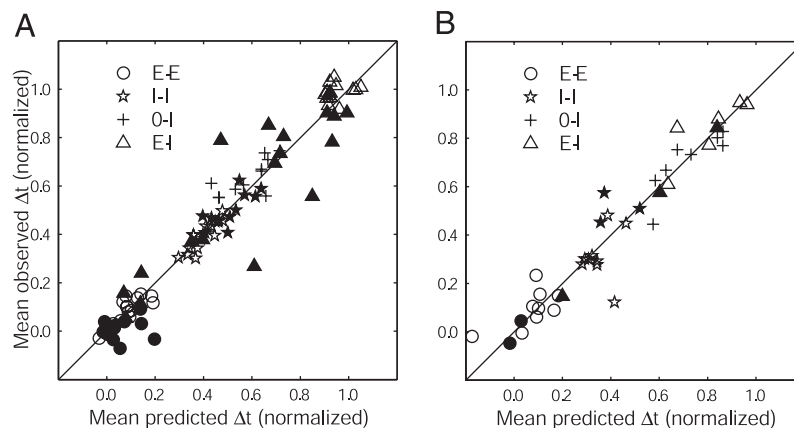


FIG. 6. Average predicted and observed spike time differences are consistent within SCs (a) and O-LM interneurons (b). Pooled results from hybrid networks made from biological neurons and virtual counterparts normalized by their unperturbed period (50–150 ms). Open circles imply E-E coupling; open stars imply I-I coupling; ‘plus’ signs imply unilateral inhibitory coupling from the virtual cell to the biological cell; and open triangles imply E-I coupling, with the biological cell giving rise to excitatory coupling. Each open symbol of a given type represents predicted and observed results from a distinct cell. Also plotted are results from paired recordings from cells connected by virtual synapses (closed circles, stars and triangles again correspond to E-E, I-I, and E-I networks, respectively). Each filled symbol represents data from a distinct paired recording. The average spike-time difference in the two-cell networks is plotted against the predicted time difference (normalized by the control ISI of the neuron), estimated from iterative simulations based on spike time response curves (STRCs). For dual-cell recordings, E-I and I-E measurements are lumped into the E-I category here, because the two cells were invariably from the same cell type, making the E-I/I-E distinction moot. Predictions correlate well with observations. Differences in all cases except two (I-I and I-O for SCs) are statistically insignificant at the $P = 0.05$ level (paired t -test), and insignificant for all cases at the $P = 0.02$ level. Predicted and observed time differences from “homogeneous” networks (E-E, I-I) cluster reliably: observed time differences, including data from both types of hybrid network, have mean \pm SD = 0.05 ± 0.06 for E-E SCs ($n = 36$), 0.08 ± 0.08 for E-E O-LMs ($n = 11$), 0.4 ± 0.08 for I-I SCs ($n = 35$), 0.4 ± 0.1 for I-I O-LMs ($n = 12$). Timing relationships in E-I networks are less reliable (0.75 ± 0.31 for E-I SCs ($n = 39$), 0.73 ± 0.25 for E-I O-LMs ($n = 9$)). This lack of reliable behavior can be seen in individual cells (cf. E-I and I-E responses in Fig. 5). For visual clarity, error bars are not included with these data. Mean values of σ (the SD of observed spike time differences, expressed as a proportion of the average interspike interval) and λ (the fraction of spike time differences that lie within $\pm 10\%$ of the mean value, expressed as a percentage of the total number of spike time differences), are as follows for each network type. For SCs: E-E, $\bar{\sigma}=0.083$, $\lambda=52\%$, $n = 10$; I-I, $\bar{\sigma}=0.084$, $\lambda=38\%$, $n = 10$; E-I, $\bar{\sigma}=0.10$, $\lambda=34\%$, $n = 17$. For O-LMs: E-E, $\bar{\sigma}=0.10$, $\lambda=48\%$, $n = 2$; I-I, $\bar{\sigma}=0.13$, $\lambda=46\%$, $n = 2$; E-I, $\bar{\sigma}=0.096$, $\lambda=43\%$, $n = 3$. Because distributions are broader in hybrid networks including two biological cells, estimates of $\bar{\sigma}$ and λ were made only from dual recordings.

Our next goal was to test the quality of “predictions” of spike time differences, based on our curve fits of STRCs, with data from both kinds of hybrid network. Figure 5 shows example data from the second type of hybrid network, constructed by coupling two, simultaneously recorded biological SCs or O-LM cells under dynamic clamp (as in Fig. 3b, but with different specific cells). Predicting behavior in these networks of two biological cells is a more rigorous test of the STR method, because fewer factors are under the experimentalist’s direct control. STRC-based predictions (black lines) are very similar to observations (gray histograms) from two-cell networks (Fig. 5), although small systematic differences render them statistically distinguishable at the $P = 0.01$ level (χ^2 test). Predictions and observations for the SC and O-LM populations are similar, despite the fact that each population is potentially mutually interconnected with peer neurons of different “sign” (excitatory or inhibitory; average predictions from a larger corpus of data are compared below). Because “cell 1” and “cell 2” were of the same cell type, one might expect E-I and I-E networks to behave identically (meaning that the I-E histogram would be a simple rotation of the E-I histogram about the point $\Delta t = 0$). Instead, E-I and I-E networks often behaved differently (see also Fig. 3b). This difference was predictable from stochastic STRCs (black lines), and comes about because E-I and I-E coupling tend to magnify small discrepancies in the details and noise levels of STRCs between the two cells. SCs and O-LM cells showed similar ranges of behavior when connected heterogeneously, sometimes showing near-synchronization (Fig. 5a, E-I; Fig. 5b, I-E; note that, the distinction between E-I and I-E is arbitrary), and sometimes showing broadly-tuned anti-synchronization (Fig. 5a, I-E; Fig. 5b, E-I).

We also analyzed the statistical “tightness” of spike-time-difference histograms, using two measures (see METHODS): σ , the estimated SD of each distribution; and λ , the percentage of spike time differences that lie near the mean value. For the pairs of SCs and O-LM cells in Fig. 5, the overall spread of the distribution (σ) does not depend strongly on the pattern of connectivity between the cells (specific values given in the legend). However, λ was larger for the E-E spike-time distributions than for I-I distributions, and for some E-I/I-E networks than for others. λ picks up features to which σ is not sensitive because these distributions are notably not Gaussian and have large tails. We compare average values of σ and λ across multiple recordings below.

Figure 6 shows summary data from experiments in SCs (Fig. 6a) and O-LM cells (Fig. 6b). The plots show the mean observed time difference in hybrid networks, plotted versus the mean time difference predicted for the same cell or pair of cells. As before, predictions come from iterative simulations based on stochastic STRCs. Both predicted and observed mean time differences have been normalized by the unperturbed firing periods used in collecting the data (100 ms for Fig. 6a, 150 ms for Fig. 6b). From these data, we draw several conclusions. First, for both SCs (Fig. 6a) and O-LM cells (Fig. 6b), predicted and observed timing differences match well, as demonstrated by the fact that most points lie near the line of identity in Fig. 6. This result, statistically quantified in the legend of Fig. 6, implies that living SCs and O-LM neurons can be modeled to first approximation as memoryless in this context, their spike times determined only by their baseline

rates and most recent synaptic input. Second, networks with homogeneous synapses (E-E, I-I) lead to consistent average timing relationships within a particular cell type (see figure legend for quantification). In contrast, networks with heterogeneous synapses (E-I) give rise to a variety of mean time differences. These results suggest that synchronization properties are uniform within each population (SCs and O-LM cells), but only with homogeneous synapses. Third, predicted and observed timing differences do not depend strongly on the type of hybrid network studied (biological/virtual versus biological/biological). This result emphasizes that our virtual neurons, modeled using a typical STRC, capture the essential behavior of neurons in this context. Fourth, mean timing differences for a given network topology are similar for SCs and O-LM cells. Both SCs and O-LM interneurons synchronize best through mutual excitation, and differences between average normalized predicted time differences for SCs and O-LM cells are statistically insignificant (as determined by a t -test, $P > 0.05$). Synchronizing mutual excitation could be monosynaptic for glutamatergic SCs, but could not for GABAergic O-LM cells without electrical synapses. Fifth, different types of hybrid networks give rise to spike-time distributions that are distinguishable in their shape, as quantified in the figure legend. Focusing on SCs, for which we have a larger data set, the average value of λ is 52% for E-E networks, but only 38% for I-I networks and 34% for E-I networks. Thus E-E networks spend a greater proportion of the time near their phase-locked solution than the other network types. E-E networks do not exhibit smaller average values of σ than I-I or E-I networks, because many of the underlying distributions have large tails that dominate the calculation of σ .

DISCUSSION

This study represents part of a new thread of work in quantitative neuroscience (DeMarse et al. 2001; Jung et al. 2001; Le Masson et al. 2002; Manor and Nadim 2001; Reyes 2003; Sharp et al. 1993), in which technology is interfaced with living neurons in an attempt to answer novel scientific questions. Because the interfaced technology can be controlled with great mathematical precision, this approach allows one to test highly quantitative hypotheses directly and specifically in living neurons and neuronal networks. Recent examples of this general approach have shown that inhibitory gain in thalamic networks can be used to functionally connect or disconnect the neocortex from the periphery (Le Masson et al. 2002), and that synchronous activity arises in multilayer feedforward neuronal networks under a wide variety of conditions (Reyes 2003). In our case, the incentive for this effort was to collect experimental data that relate directly to well understood reduced models used in nonlinear dynamical analyses of synchronization. These models allow us to understand the behavior of large networks in terms of a small number of modeled elements. The desired end goal of this effort is a verifiable, mechanistic theory of how neuronal synchronization arises within and between hippocampal substructures. Our success in predicting network timing relationships, based on simple measurements from single cells, makes us optimistic that this goal is achievable.

Our recordings from SCs and O-LM interneurons indicate that these cells can synchronize, with nearly zero phase lag, via mutual excitation, but that they phase lock in anti-synchrony

via mutual inhibition. It is no coincidence that these two states are the most common ones we see. It can be proven mathematically that coupled neurons with identical properties and symmetric, instantaneous and pulsatile coupling have these two phase-locked solutions (Ermentrout 1996; Ermentrout and Kopell 1991; Hansel et al. 1995), although the solutions are not necessarily mathematically stable. Complications like nonpulsatile synaptic coupling and cellular heterogeneity distort these relationships, often moving phase-locked states away from perfect synchrony or anti-synchrony and sometimes changing the stability of these states (Ermentrout 1996; Ermentrout and Kopell 1991; Hansel et al. 1995; White et al. 1998a).

Our result that mutual inhibition does not lead to stable synchrony seems to contrast with a number of modeling studies of spiking neurons (Ermentrout 1996; Hansel et al. 1995; Van Vreeswijk et al. 1994). Two potentially overlapping factors may contribute to resolving this apparent contradiction. First, model neurons with prominent slow conductances give rise to STRCs that are much like our measured curves and give very similar predictions (Acker et al. 2003; Crook et al. 1998; Ermentrout et al. 2001). Both SCs (Dickson et al. 2000) and O-LM interneurons (Maccaferri and McBain 1996) express large amounts of the slow, hyperpolarization-activated cation current I_h , thought to contribute to the intrinsic theta rhythmicity of the two populations (Dickson et al. 2000; Gillies et al. 2002; White et al. 1995). Second, in modeling studies, inhibition-based synchronization often has a small domain of attraction that the network may escape from under noisy conditions (Acker et al. 2003).

The similar STR relationships for MEC SCs and CA1 O-LM interneurons have interesting implications for oscillations in the true biological network. Both SCs (Germroth et al. 1991; Klink and Alonso 1997; Lingenhöhl and Finch 1991) and O-LM cells (M. Whittington, personal communication) give rise to local axonal collaterals, implying that there may be reciprocal interconnections within each population. For a pool of monosynaptically connected excitatory SCs, we would predict robust synchronization at theta frequencies. For a pool of monosynaptically connected inhibitory O-LM cells, we would predict that synchronization in phase is not possible at theta frequencies. It should be noted that electrical synapses have recently been identified in this population, which potentially could stabilize the synchronous state (Zhang et al. 2004). Alternatively, synchrony of O-LM cells would require involvement of another neuronal population, as has been seen in simulations (Rotstein et al. 2003).

Predicted and observed phase differences were more consistent in homogeneous (E-E, I-I) networks than in heterogeneous (E-I, 0-I) networks, as indicated by the spread of observed spike time differences from recording to recording (quantified in the legend of Fig. 6). This difference can be traced to the mathematical structures that underlie STR methods. As mentioned above, homogenous networks tend to exhibit near-synchronous or near-anti-synchronous phase-locked solutions (Ermentrout 1996; Ermentrout and Kopell 1991; Hansel et al. 1995). Thus predicted and observed phase relationships in homogeneous networks are not sensitive to small amounts of variation in the properties of individual cells. In contrast, predicted and observed outcomes in networks with heterogeneous coupling depend more sensitively on the detailed properties of individual neurons.

We also see clear trends in the “tightness” of distributions of spike time differences for networks of different types. Pairs of SCs spend more time near their “preferred” (average) state in the E-E case than in the I-I or E-I case, as measured by λ . Such differences in the shape of spike-time-difference distributions are predictable from measurement of STRCs (Fig. 5), and reflect the differences in the attractiveness of phase-locked states for different types of networks. In general, we find that the SD σ of the distributions does not depend on the type of network. We conclude that commonly arising long tails of spike-time-difference distributions – generated by noise, phase-slipping and other causes – imply that the “typical” distance of Δt from its average value is insensitive to network type, even while the proportion of time spent near the average Δt depends strongly on the network.

Homogeneous (E-E, I-I) and heterogeneous (E-I, 0-I) networks also differed in terms of consistency of mean time differences measured from case to case (Fig. 6). In homogeneous networks, mean time differences were remarkably consistent. This result surprised us, given that neurons within a defined population often behave differently, and that small differences in parameters can lead to large differences in spike timing in modeling studies (Acker et al. 2003). The consistency we observed within a large number of recordings may indicate that synchronization properties are actively conserved within a cell type. Heterogeneous networks show less consistent timing relationships, implying again that small differences in cellular properties can lead to unpredictable behavior in these less-stable networks.

Strictly speaking, our STR techniques only predict network behavior for two-cell networks with fixed synaptic strengths and synaptic kinetics. However, synchronization properties among entorhinal stellate cells (SCs) are largely independent of synaptic strength and kinetics (Fig. 4), implying that only the degree of synchronization would be affected by factors like short-term synaptic plasticity but not the form. For example, progressive depression of mutual excitatory synapses in a pool of SCs would only be expected to gradually increase the amount of “jitter” around the synchronized state (Fig. 4a). Predicted network properties were only observed to change under one condition: inhibition with very slow synapses (Fig. 4b, bottom-right panel). This effect of synchronization via slow inhibition arose because early ($t < 20$ ms) slow inhibitory inputs led to slight average delays in spike timing, and late ($t > 80$ ms) inputs led, on average, to no change in spike timing. Late inputs probably have no effect on the following spike because they rise too slowly to affect its timing. The delaying effect of early slow inputs is more surprising, given the results we see for faster inhibition, and demonstrates how subtle the interactions of synaptic and intrinsic conductances can be.

The “small networks” approach used here generalizes well to describe larger networks, at least those with all-to-all connections (Acker et al. 2003; White et al. 1998a). Under the right conditions, STR methods extend to handle further complexities. For example, if individual synapses are small enough that their effects on STRCs combine linearly, our experiments as designed can account for the effects of unsynchronized barrages of presynaptic activity on postsynaptic spike timing (and, consequently, network phase locking) (Ermentrout and Chow 2002). Even without the assumption of linearity, the STR method can be extended to account for behavior in

complex networks from measurements on single neurons (Ermentrout and Kopell 1998; Rotstein et al. 2003). For example, the stability of y -intercepts of STRCs can predict whether a single member of a large, synchronous pool will be attracted back into synchronous state after being perturbed away. STRCs are also useful for describing the interactions of two or more “clusters” of neurons with intra-cluster synchrony.

ACKNOWLEDGMENTS

We thank M. Beck, B. G. Burton, G. B. Ermentrout, K. Josic, J. Ritt, H. Rotstein, and M. Whittington for helpful discussions and advice. J. Bettencourt provided invaluable programming assistance.

GRANTS

This work was supported by National Institutes of Health Grants R01 NS-34425 to J. A. White, R01 NS-46058 to N. Kopell, R01 DC-006013 to M. I. Banks, and F32 MH-066555 to T. I. Netoff. Instrumentation development was supported by National Science Foundation Grant BES 0085177 to J. A. White.

REFERENCES

- Acker CD, Kopell N, and White JA.** Synchronization of strongly coupled excitatory neurons: relating network behavior to biophysics. *J Comput Neurosci* 15: 71–90, 2003.
- Alonso A and Klink R.** Differential electroresponsiveness of stellate and pyramidal-like cells of medial entorhinal cortex layer II. *J Neurophysiol* 70: 128–143, 1993.
- Alonso A and Llinás RR.** Subthreshold Na^+ -dependent theta-like rhythmicity in stellate cells of entorhinal cortex layer II. *Nature* 342: 175–177, 1989.
- Berretta N and Jones RS.** A comparison of spontaneous EPSCs in layer II and layer IV–V neurons of the rat entorhinal cortex in vitro. *J Neurophysiol* 76: 1089–1100, 1996.
- Bragin A, Engel J Jr, Wilson CL, Fried I, and Mathern GW.** Hippocampal and entorhinal cortex high-frequency oscillations (100–500 Hz) in human epileptic brain and in kainic-acid-treated rats with chronic seizures. *Epilepsia* 40: 127–137, 1999.
- Burchell TR, Faulkner HJ, and Whittington MA.** Gamma frequency oscillations gate temporally coded afferent inputs in the rat hippocampal slice. *Neurosci Lett* 255: 151–154, 1998.
- Canavier CC, Butera RJ, Dror RO, Baxter DA, Clark JW, and Byrne JH.** Phase response characteristics of model neurons determine which patterns are expressed in a ring circuit model of gait generation. *Biol Cybern* 77: 367–380, 1997.
- Chow CC, White JA, Ritt J, and Kopell N.** Frequency control in synchronized networks of inhibitory neurons. *J Comput Neurosci* 5: 407–420, 1998.
- Chrobak JJ and Buzsáki G.** Gamma oscillations in the entorhinal cortex of the freely behaving rat. *J Neurosci* 18: 388–398, 1998.
- Crook SM, Ermentrout GB, and Bower JM.** Spike frequency adaptation affects the synchronization properties of networks of cortical oscillations. *Neural Comput* 10: 837–854, 1998.
- DeMarse TB, Wagenaar DA, Blau AW, and Potter SM.** The neurally controlled animat: biological brains acting with simulated bodies. *Auton Robot* 11: 305–310, 2001.
- Demir SS, Butera RJ Jr, DeFranceschi AA, Clark JW Jr, and Byrne JH.** Phase sensitivity and entrainment in a modeled bursting neuron. *Biophys J* 72: 579–594, 1997.
- Dickson CT, Magistretti J, Shalinsky MH, Fransen E, Hasselmo ME, and Alonso A.** Properties and role of $I(h)$ in the pacing of subthreshold oscillations in entorhinal cortex layer II neurons. *J Neurophysiol* 83: 2562–2579, 2000.
- Dorval AD, Christini DJ, and White JA.** Real-Time linux dynamic clamp: a fast and flexible way to construct virtual ion channels in living cells. *Ann Biomed Eng* 29: 897–907, 2001.
- Eckert WA 3rd, Willcockson HH, and Light AR.** Interference of biocytin with opioid-evoked hyperpolarization and membrane properties of rat spinal substantia gelatinosa neurons. *Neurosci Lett* 297: 117–120, 2001.
- Ermentrout B.** Type I membranes, phase resetting curves, and synchrony. *Neural Comput* 8: 979–1001, 1996.
- Ermentrout GB and Chow CC.** Modeling neural oscillations. *Physiol Behav* 77: 629–633, 2002.
- Ermentrout GB and Kopell N.** Multiple pulse interactions and averaging in systems of coupled neural oscillators. *J Math Biol* 29: 195–217, 1991.
- Ermentrout GB and Kopell N.** Fine structure of neural spiking and synchronization in the presence of conduction delays. *Proc Natl Acad Sci USA* 95: 1259–1264, 1998.
- Ermentrout B, Pascal M, and Gutkin B.** The effects of spike frequency adaptation and negative feedback on the synchronization of neural oscillators. *Neural Comput* 13: 1285–1310, 2001.
- Fellous JM and Sejnowski TJ.** Cholinergic induction of oscillations in the hippocampal slice in the slow (0.5–2 Hz), theta (5–12 Hz), and gamma (35–70 Hz) bands. *Hippocampus* 10: 187–197, 2000.
- Fransen E, Alonso AA, and Hasselmo ME.** Simulations of the role of the muscarinic-activated calcium-sensitive nonspecific cation current INCM in entorhinal neuronal activity during delayed matching tasks. *J Neurosci* 22: 1081–1097, 2002.
- Freund TF and Buzsáki G.** Interneurons of the hippocampus. *Hippocampus* 6: 347–470, 1996.
- Fries P, Roelfsema PR, Engel AK, Konig P, and Singer W.** Synchronization of oscillatory responses in visual cortex correlates with perception in interocular rivalry. *Proc Natl Acad Sci USA* 94: 12699–12704, 1997.
- Germroth P, Schwerdtfeger WK, and Buhl EH.** Ultrastructure and aspects of functional organization of pyramidal and nonpyramidal entorhinal projection neurons contributing to the perforant path. *J Comp Neurol* 305: 215–231, 1991.
- Gillies MJ, Traub RD, LeBeau FE, Davies CH, Gloveli T, Buhl EH, and Whittington MA.** A model of atropine-resistant theta oscillations in rat hippocampal area CA1. *J Physiol* 543: 779–793, 2002.
- Gloor P.** *The Temporal Lobe and Limbic System.* New York: Oxford, 1997.
- Gray CM, Konig P, Engel AK, and Singer W.** Oscillatory responses in cat visual cortex exhibit inter-columnar synchronization which reflects global stimulus properties. *Nature* 338: 334–337, 1989.
- Hansel D, Mato G, and Meunier C.** Synchrony in excitatory neural networks. *Neural Comput* 7: 307–337, 1995.
- Hasselmo ME, Fransen E, Dickson C, and Alonso AA.** Computational modeling of entorhinal cortex. *Ann NY Acad Sci* 911: 418–446, 2000.
- Hinkle DJ and Macdonald RL.** Beta subunit phosphorylation selectively increases fast desensitization and prolongs deactivation of $\alpha 1\beta 1\gamma 2L$ and $\alpha 1\beta 3\gamma 2L$ GABA(A) receptor currents. *J Neurosci* 23: 11698–11710, 2003.
- Jonas P.** The time course of signaling at central glutamatergic synapses. *News Physiol Sci* 15: 83–89, 2000.
- Jung R, Brauer EJ, and Abbas JJ.** Real-time interaction between a neuro-morphic electronic circuit and the spinal cord. *IEEE Trans Neural Syst Rehabil Eng* 9: 319–326, 2001.
- Klink R and Alonso A.** Morphological characteristics of layer II projection neurons in the rat medial entorhinal cortex. *Hippocampus* 7: 571–583, 1997.
- Konopacki J, MacIver MB, Bland BH, and Roth SH.** Carbachol-induced EEG “theta” activity in hippocampal brain slices. *Brain Res* 405: 196–198, 1987.
- Kopell N and Ermentrout GB.** Mechanisms of phase-locking and frequency control in pairs of coupled neural oscillators. In: *Handbook on Dynamical Systems*, edited by Fiedler B. New York: Elsevier, 2002, p. 3–54.
- Le Masson G, Renaud-Le Masson S, Debay D, and Bal T.** Feedback inhibition controls spike transfer in hybrid thalamic circuits. *Nature* 417: 854–858, 2002.
- Lingenhöhl K and Finch DM.** Morphological characterization of rat entorhinal neurons in vivo: soma-dendritic structure and axonal domains. *Exp Brain Res* 84: 57–74, 1991.
- Lytton WW and Sejnowski TJ.** Simulations of cortical pyramidal neurons synchronized by inhibitory interneurons. *J Neurophysiol* 66: 1059–1079, 1991.
- Maccacferri G and McBain CJ.** The hyperpolarization-activated current (I_h) and its contribution to pacemaker activity in rat CA1 hippocampal stratum oriens-alveus interneurons. *J Physiol* 497: 119–130, 1996.
- Manor Y and Nadim F.** Synaptic depression mediates bistability in neuronal networks with recurrent inhibitory connectivity. *J Neurosci* 21: 9460–9470, 2001.
- Markram H, Wang Y, and Tsodyks M.** Differential signaling via the same axon of neocortical pyramidal neurons. *Proc Natl Acad Sci USA* 95: 5323–5328, 1998.
- Oprisan SA and Canavier CC.** Stability analysis of rings of pulse-coupled oscillators: the effect of phase-resetting in the second cycle after the pulse is important at synchrony and for long pulses. *Differential Equat Dynamical Systems* 9: 243–258, 2001.

- Oprisan SA and Canavier CC.** The influence of limit cycle topology on the phase resetting curve. *Neural Comput* 14: 1027–1057, 2002.
- Oprisan SA, Thirumalai V, and Canavier CC.** Dynamics from a time series: can we extract the phase resetting curve from a time series? *Biophys J* 84: 2919–2928, 2003.
- Pike FG, Goddard RS, Suckling JM, Ganter P, Kasthuri N, and Paulsen O.** Distinct frequency preferences of different types of rat hippocampal neurons in response to oscillatory input currents. *J Physiol* 529: 205–213, 2000.
- Reyes AD.** Synchrony-dependent propagation of firing rate in iteratively constructed networks in vitro. *Nat Neurosci* 6: 593–599, 2003.
- Reyes AD and Fetz EE.** Two modes of interspike interval shortening by brief transient depolarizations in cat neocortical neurons. *J Neurophysiol* 69: 1661–1672, 1993.
- Robinson HP and Kawai N.** Injection of digitally synthesized synaptic conductance transients to measure the integrative properties of neurons. *J Neurosci Methods* 49: 157–165, 1993.
- Roelfsema PR, Engel AK, Konig P, and Singer W.** Visuomotor integration is associated with zero time-lag synchronization among cortical areas. *Nature* 385: 157–161, 1997.
- Rotstein H, Clewley R, Gillies M, Acker CD, White JA, Whittington MA, and Kopell N.** Slow and fast inhibition and h-current interact to create a theta rhythm in CA1 in vitro. *Soc Neurosci Abstr* 31: 258.253, 2003.
- Schlosser B, ten Bruggencate G, and Sutor B.** The intracellular tracer Neurobiotin alters electrophysiological properties of rat neostriatal neurons. *Neurosci Lett* 249: 13–16, 1998.
- Sharp AA, O'Neil MB, Abbott LF, and Marder E.** Dynamic clamp: computer-generated conductances in real neurons. *J Neurophysiol* 69: 992–995, 1993.
- Spruston N, Jaffe DB, and Johnston D.** Dendritic attenuation of synaptic potentials and currents: the role of passive membrane properties. *Trends Neurosci* 17: 161–166, 1994.
- Stoop R, Schindler K, and Bunimovich LA.** Neocortical networks of pyramidal neurons: from local locking and chaos to macroscopic chaos and synchronization. *Nonlinearity* 13: 1515–1529, 2000.
- Thomson AM and Deuchars J.** Temporal and spatial properties of local circuits in neocortex. *Trends Neurosci* 17: 119–126, 1994.
- Traub RD, Jefferys JGR, and Whittington MA.** *Fast Oscillations in Cortical Circuits*. Cambridge, MA: MIT Press, 1999.
- Traub RD, Whittington MA, Stanford IM, and Jefferys JG.** A mechanism for generation of long-range synchronous fast oscillations in the cortex. *Nature* 383: 621–624, 1996.
- Van Vreeswijk C, Abbott LF, and Ermentrout GB.** When inhibition not excitation synchronizes neural firing. *J Comput Neurosci* 1: 313–321, 1994.
- White JA, Budde T, and Kay AR.** A bifurcation analysis of neuronal subthreshold oscillations. *Biophys J* 69: 1203–1217, 1995.
- White JA, Chow CC, Ritt J, Soto-Trevino C, and Kopell N.** Synchronization and oscillatory dynamics in heterogeneous, mutually inhibited neurons. *J Comput Neurosci* 5: 5–16, 1998a.
- White JA, Klink R, Alonso A, and Kay AR.** Noise from voltage-gated ion channels may influence neuronal dynamics in the entorhinal cortex. *J Neurophysiol* 80: 262–269, 1998b.
- Whittington MA, Traub RD, and Jefferys JG.** Synchronized oscillations in interneuron networks driven by metabotropic glutamate receptor activation. *Nature* 373: 612–615, 1995.
- Wilson M and Bower JM.** Cortical oscillations and temporal interactions in a computer simulation of piriform cortex. *J Neurophysiol* 67: 981–995, 1992.
- Winfree AT.** *The Geometry of Biological Time*. New York: Springer, 2001.
- Winson J.** Loss of hippocampal theta rhythm results in spatial memory deficit in the rat. *Science* 201: 160–163, 1978.
- Xi XZ and Xu ZC.** The effect of neurobiotin on membrane properties and morphology of intracellularly labeled neurons. *J Neurosci Methods* 65: 27–32, 1996.
- Ylinen A, Bragin A, Nadasdy Z, Jando G, Szabo I, Sik A, and Buzsaki G.** Sharp wave-associated high-frequency oscillation (200 Hz) in the intact hippocampus: network and intracellular mechanisms. *J Neurosci* 15: 30–46, 1995.
- Zhang X-L, Zhang L, and Carlen PL.** Electrotonic coupling between stratum oriens interneurons in the intact in vitro mouse juvenile hippocampus. *J Physiol* 558: 825–839, 2004.